AIAA JOURNAL
Vol. 30, No. 9, September 1992

Crossflow Vortex and Transition Measurements by Use of Multielement Hot Films

Naval K. Agarwal*
Analytical Services and Materials, Inc., Hampton, Virginia 23666
Dal V. Maddalon†
NASA Langley Research Center, Hampton, Virginia 23665
Siva M. Mangalam‡
Analytical Services and Materials, Inc., Hampton, Virginia 23666
and
Fayette S. Collier Jr.§
NASA Langley Research Center, Hampton, Virginia 23665

An experiment on a 45-deg swept wing was conducted to study three-dimensional boundary-layer characteristics using surface-mounted, microthin, multielement hot-film sensors. A large hot-film gauge was fabricated that combined three arrays of 64 crossflow sensors each and a single array of 32 transition sensors. Two such gauges were mounted along the model chord. Crossflow vortex structure and boundary-layer transition were measured from the simultaneously acquired signals of the hot films. Stationary and nonstationary crossflow disturbances were measured from hot-film sensor arrays. Spanwise variation of the root-mean-square hot-film signal show a local minima and maxima. The distance between two minima corresponds to the stationary crossflow vortex wavelength and agrees with naphthalene flow-visualization results. The chordwise and spanwise variation of amplified traveling (nonstationary) crossflow disturbance characteristics were measured as Reynolds number was varied. The frequency of the most amplified crossflow disturbances agrees with linear stability theory.

Nomenclature

C = chord length, 1829 mm
C_p = surface pressure coefficient
e = hot-film signal, V
e' = root mean square of signal, V
f_c = amplified crossflow disturbance frequency
$f_{c_{\max}}$ = maximum amplified crossflow disturbance frequency
R_c = chord Reynolds number
t = time, s
U_o = freestream velocity
$u'v'w'$ = perturbations in X, Y, and Z directions, respectively
X, Y, Z = streamwise (chordwise), normal, and spanwise coordinates, respectively
λ = crossflow vortex wavelength, mm

Introduction

THE attainment of laminar flow on aircraft wings has significant potential for reducing drag and increasing fuel efficiency. One aspect of drag reduction technology involves the avoidance or delay of laminar boundary-layer transition to turbulent flow by controlling the growth of boundary-layer disturbances.[1] For wings with moderate leading-edge sweep angles, the flow is highly three dimensional and the boundary-layer transition may be strongly influenced by the presence of crossflow vortices and other boundary-layer disturbances. Comprehensive reviews of both theoretical and experimental studies on three-dimensional boundary-layer instabilities and transition are given by Reed and Saric,[2] Saric,[3] and Arnal.[4] The presence of highly amplified instabilities in the boundary layer is known to initiate transition of the laminar boundary layer to turbulent flow for large Reynolds numbers.[5-10]

Kohama[10] studied the crossflow instability on a rotating disk where the flowfield is similar to the flow over a swept wing. Both flowfields involve instabilities due to the inflectional nature of the crossflow velocity profile. Poll[11] studied the effect of crossflow instability upon transition on a swept cylinder. Recent wind-tunnel experiments on the crossflow vortex problem include those of Saric and Yeates,[5] Bippes and Nitschke-Kowsky,[6] Arnal and Juillen,[7] Muller and Bippes,[8] Dagenhart et al.,[9] and Mangalam et al.[12]

Dagenhart et al. and Mangalam et al. report measurements of crossflow vortices on a 45-deg swept-wing model. Dagenhart et al. observed stationary crossflow vortices through flow visualization studies using sublimating chemicals. Mangalam et al. reported hot-film measurements at one chord location to obtain crossflow vortex characteristics. In this paper, more detailed measurements are reported on the same 45-deg swept-wing model tested at the Arizona State University (ASU) wind tunnel (same facility as used by Dagenhart et al,[9] and Mangalam et al.[12]). Stationary and nonstationary crossflow disturbances were studied using simultaneous measurements from multielement sensors located at several chordwise locations. Stationary crossflow vortex wavelength was determined by a flow-visualization method and from the rms of the spanwise located multielement hot-film sensors.

Test Apparatus and Instrumentation

The ASU unsteady wind tunnel is a closed-circuit tunnel with a 1.4-m-square and 5-m-long test section. The tunnel can

---

Presented as Paper 91-0166 at the AIAA 29th Aerospace Sciences Meeting, Reno, NV, Jan. 7-10, 1991; received June 28, 1991; revision received Jan. 22, 1992; accepted for publication Feb. 4, 1992.

*Senior Scientist. Associate Fellow AIAA.

†Technical Manager, Laminar Flow Control Project Office.

‡Vice President. Member AIAA.

§Head, Laminar Flow Control Project Office. Member AIAA.

be used as an unsteady wind tunnel, in which oscillating flows of air can be generated, and can also be used as a conventional steady-flow low-turbulence wind tunnel. For the present experiments, the wind tunnel was operated in the latter mode with a maximum steady freestream velocity of 35 m/s. The tunnel has an aluminum honeycomb and seven turbulence-damping screens in the 2.7- × 3.6-m settling chamber. The contraction cone employs a fifth-degree polynomial shape with a length to diameter ratio of 1.25 and a contraction ratio of 5.33. A 150-hp variable-speed dc motor and single-stage axial fan produce test Reynolds numbers (based on wing chord length) up to about 3.8×10^6.

The test model consists of an NLF(2)-0415 airfoil (Fig. 1), mounted at an angle-of-attack of about − 4 deg. Contoured tunnel-wall liners are used to simulate infinite swept-wing flow (Fig. 2). The model is mounted vertically with the wing leading edge swept back at 45 deg and has two rows of streamwise pressure orifices. This test setup, i.e., model with a small negative angle of attack, produces a long run of crossflow dominated flow. With this configuration, the pressure gradient is favorable to about $X/C = 0.71$ (Fig. 3). The wind tunnel and model are described in detail by Saric et al.[13] The important features are that the freestream v' and w' fluctuations are around 0.04% U_o and the u' fluctuations are around 0.09% U_o, The higher u' value is due to very low-frequency pressure fluctuations in the tunnel.

A PC-based digital data acquisition and instrumentation system (DAISy) was used for data acquisition. The DAISy contains a custom-built data acquisition card with eight independent analog-to-digital converters, with 32 kHz throughput each, and 16 input channels. Each channel has its own signal conditioning card that provides both gain and antialiasing filtering functions. Sixteen constant temperature anemometers were used. The DAISy software allowed the simultaneous acquisition of any eight selected channels from the 16 connected sensors. Data files were recorded on the 360 Mb optical disk and were later transferred to and processed on a CRAY-2S supercomputer. Spectral results were averaged for at least 30 records (5 s or more) to get the required statistical accuracy.

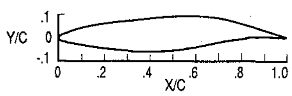

Fig. 1 Airfoil geometry.

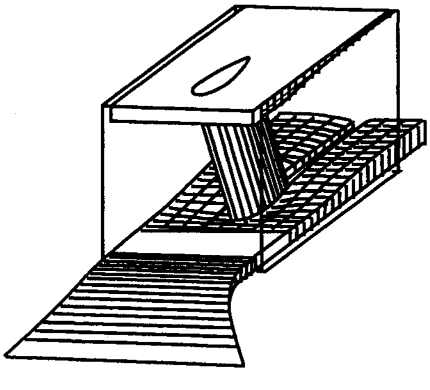

Fig. 2 Schematic diagram of model in tunnel.

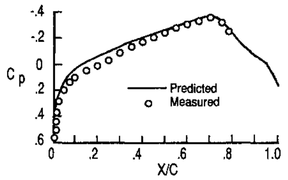

Fig. 3 Airfoil pressure distribution.[9]

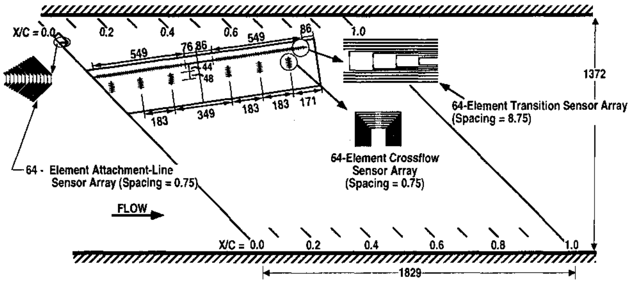

Fig. 4 Location of multielement sensor arrays on wing model (dimensions in mm).

Multielement films (MEF) have been utilized at NASA Langley Research Center to study boundary-layer transition and separation at speeds ranging from subsonic to low supersonic.[9,12,14-19] The surface-mounted, microthin, multielement hot-film sensors used in the present experiment were designed and fabricated at the NASA Langley Research Center. These sensors were formed by vapor deposition of layers of nickel and copper on a 50-μm-thick Kapton sheet. Initially, a 60-element transition sensor array (sensor size = 0.125 × 1.145 mm) and a 33-element crossflow sensor array were used. The 60-element transition sensor array covered the model chordwise from $X/C = 0.52$ to 0.60; sensor elements were aligned approximately perpendicular to the vortex streaks as observed from the sublimating chemical (naphthalene) flow-visualization technique. A 33-element sensor array was used to measure the spanwise crossflow vortex development. The crossflow sensor array covered a spanwise distance of 25 mm, and the sensors were aligned normal to the crossflow vortex pattern as obtained by the flow visualization.

In this paper, additional analysis was made of the data reported in Ref. 12. Also, a second wind-tunnel entry was later made that used more advanced sensor configurations. One configuration combined three chordwise arrays—each with 64 crossflow sensors and one array of 32 transition sensors. Two such gauges were very carefully joined (see Fig. 4), and the joint was polished with a fine emery paper. The naphthalene flow visualization confirmed that there was no local disturbance at the joint. This hot-film sensors configuration enabled measurements of crossflow vortices at six chordwise ($X/C = 0.04$, 0.15, 0.26, 0.45, 0.56, and 0.67) locations. The transition sensors array covered about 0.80 chord length. A 64-element attachment-line sensor array (Fig. 4) was wrapped around the leading edge of the model. Flow-visualization tests were made before and after the sensor arrays were installed to ensure that the edges of the film did not trip the boundary layer and that the presence of the sensor arrays did not alter the test flow.

The nominal cold resistance of each of the sensors was about 5Ω with a maximum variation of about ± 0.2Ω. Flat ribbon cables were soldered to leads from each sensor and routed through model ports. Ribbon cables were connected to coaxial cables (through a D-type connector) that, in turn, were wired to constant temperature anemometers (CTA). Care was taken to ensure that connecting wires did not interfere with the flow characteristics at the test regions. All of the sensor elements were operated at a nominal overheat ratio of 1.2. The sensors were uncalibrated and the overheat and offset voltages for each sensor (connected to a CTA) were carefully adjusted such that each sensor was at nearly the same operating conditions.

Signals from the 64-element attachment-line sensor array indicated that the attachment-line flow was laminar to the maximum test Reynolds number. The leading-edge geometry and test conditions did not induce any attachment-line contamination.

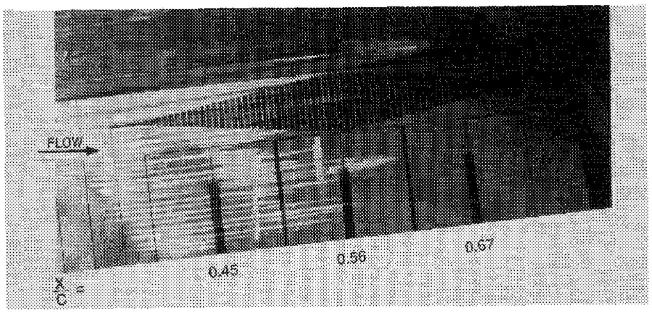

Fig. 5 Crossflow vortex visualization using naphthalene, $R_c = 2.0 \times 10^6$.

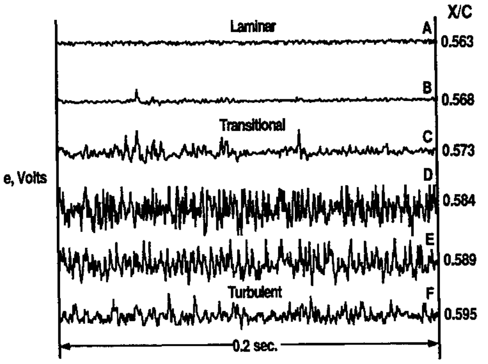

Fig. 6 Simultaneously acquired signals from 60-element transition sensor array, $R_c = 2.15 \times 10^6$.

Flow Visualization

The surface flow characteristics were visualized using a sublimating chemical technique. A naphthalene spray placed a white sublimating coating over the painted black wing surface. The naphthalene sublimated faster in the high-shear regions, which revealed the stationary crossflow vortices as alternating black and white streaks. The transition region is indicated by a sawtooth pattern, and the stationary crossflow vortex streaks are clearly shown in Fig. 5 for a Reynolds number of 2×10^6. The distance between dark and white streaks (crossflow vortex wavelength) did not vary in the chordwise direction $0.2 \leq X/C \leq 0.6$, for the range of measurement with hot films and flow visualization. The flow-visualization pattern observed in the present tests was similar to that observed by Dagenhart et al.[9]

Transition

Transition location can be determined by raw hot-film signals, by the rms of the signal versus X/C, by the spectral content of the signal, and by the flow intermittency factor (defined as the fraction of the total time that the flow is turbulent and independent of sensor calibration) vs X/C. In this work, all of these methods were used to determine when the boundary layer became transitional and turbulent.

Boundary-layer state from the time series plot is shown in Fig. 6 for $R_c = 2.15 \times 10^6$. The traces are reconstructed from the hot-film signals located at different chordwise locations and sampled at 10 kHz. To the extent possible, sensors were operated at the same overheat ratios, and the error in rms was not more than ± 7–8%. The flow is mostly laminar at $X/C = 0.563$ with some turbulent spikes appearing at $X/C = 0.568$. The frequency of the spikes increase at $X/C = 0.573$ where transitional flow is observed and the flow intermittency is about 0.5. At $X/C = 0.584$, the flow is mostly turbulent. At $X/C = 0.595$, the flow is fully turbulent. The boundary-layer state from $X/C = 0.563$ to 0.595 is marked by the letters A–F in the rms and intermittency plots for $R_c = 2.15 \times 10^6$ in Figs. 7 and 8, respectively.

The rms of the hot-film signal with chordwise distance is shown in Fig. 7 for $R_c = 2\text{–}2.6 \times 10^6$. The sharp rise in the rms of the signal is taken as the beginning of transition. After reaching a peak level, the rms drops to a value corresponding to fully turbulent flow. At this spanwise location, the flow remains laminar for $R_c \leq 2.0 \times 10^6$ and is turbulent for $R_c \geq 2.6 \times 10^6$ for the range of chord length covered by the transition sensor array. The intermittency factor for the data of Fig. 7 is shown in Fig. 8. The flow intermittency factor was computed from hot-film time series using a method similar to the one described by Narasimha.[20] The intermittency factor plots are similar to the rms curves of Fig. 7 (the fully turbulent state has an intermittency factor of 1).

The data presented in Figs. 6–8 are for one spanwise location, and the variation of transition in the spanwise direction was studied only by flow visualization. Figure 9 shows the transition summary results obtained from the data of Figs. 7 and 8 (location F). For $R_c \geq 2.15 \times 10^6$, the transition location is ahead of the minimum pressure location, i.e., $X/C = 0.71$ (Fig. 3). This and flow-visualization results suggest that transition is induced by the crossflow instabilities caused by the sweep of the model. Multielement hot-film and flow-visualization results of Dagenhart et al.[9] are also shown in Fig. 9, and they show good agreement with the present multielement hot-film results within the range of experimental accuracy.

Crossflow Vortices

Crossflow vortices, which are characterized by rotation in the same direction, are the result of the inflectional nature of the crossflow velocity profile.[21,22] Within the boundary layer, the crossflow velocity profile has a maximum at some distance from the wing surface and is zero at the wing surface and at the boundary-layer edge. Mack[23] and Poll[11] present a detailed description of the crossflow instability. Poll experimentally studied the flow over a yawed cylinder. Malik and Poll[24] theoretically studied the flow over a yawed cylinder including curvature effects. Crossflow instability can be characterized as 1) a stationary disturbance with regularly spaced vortices that can be seen on the surface by a flow visualization technique,

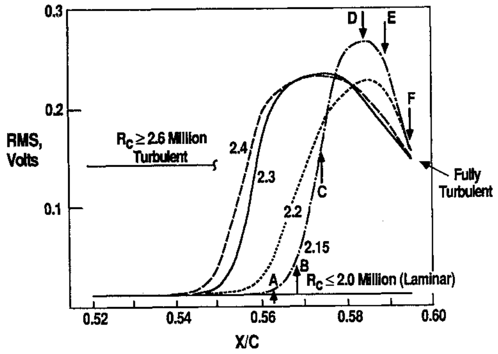

Fig. 7 Chordwise variation of rms signal from 60-element transition sensor array.

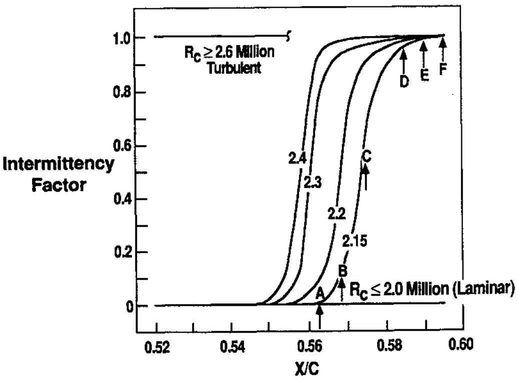

Fig. 8 Chordwise variation of intermittency factor from 60-element transition sensor array.

and 2) a nonstationary or traveling disturbance characterized by large-amplitude harmonics, as evidenced by sharp peaks in the spectra. These flow instabilities may lead to an early transition, as discussed in the preceding section.

Michel et al.[25] conducted a hot-wire experiment on a swept-wing model for which they measured the spanwise variation of crossflow instabilities. Bippes and Nitschke-Kowsky[6] used a swept flat plate to show that the frequency of the most amplified nonstationary disturbance was dependent on Reynolds number. Saric and Yeates[5] made detailed hot-wire measurements in the spanwise (and chordwise) direction at a constant distance from the wing surface to show a large spanwise rms variation. Their hot-wire measurements (at maximum crossflow velocity location) measured a crossflow wavelength of 5 mm, whereas their flow-visualization results indicated a wavelength of 10 mm. Using the actual test conditions of this experiment, Reed[26] expressed the difference in wavelength as "crossflow/crossflow interactions." Reed showed that it is possible for a parametric resonance to occur between a previously amplified (according to linear theory) 5-mm vortex and a presently amplified 10-mm vortex and that measurements taken near the maximum crossflow velocity would show a strong periodicity of 5 mm. Reed's calculations showed that the 5-mm periodicity dies out near the wall and that the 10-mm periodicity dominates there. Kohama[10] experimentally studied three-dimensional boundary-layer transition on an axisymmetric rotating body and concluded that traveling waves were induced by stationary disturbances. Similar to Saric and Yeates,[5] Kohama's hot-wire measurements noted that a discrepancy exists between the frequency and, hence, the wavelength of the disturbances from the hot-wire and flow-visualization results. He noted that, as the disturbances develop into more than single-curled vortices, then the hot-wire signal should begin to include frequencies from higher harmonics and periodicity of them should rapidly disappear. From the near wall measurements of Saric and Yeates[5] and Kohama,[10] it is inferred that surface hot-films measurements should show a maximum near the high-shear region and a minimum near the low-shear region between two corotating crossflow vortices, as shown schematically in Fig. 10. Dashed vortices are the counter-rotating portion of the fundamental disturbance that disappear near the wall, as explained by Reed.[26] High-shear points occur where flow is directed toward the surface by both vortices, and lower-shear points are found where both vortices direct flow away from the surface. The high- and low-shear values are due to u' perturbations caused by the very weak, but fundamental, vortex components v' and w'. As compared to a hot wire mounted off the surface, a surface-mounted, multielement hot-film should give a more direct measurement of the crossflow vortex wavelength similar to the wavelength obtained by flow visualization.

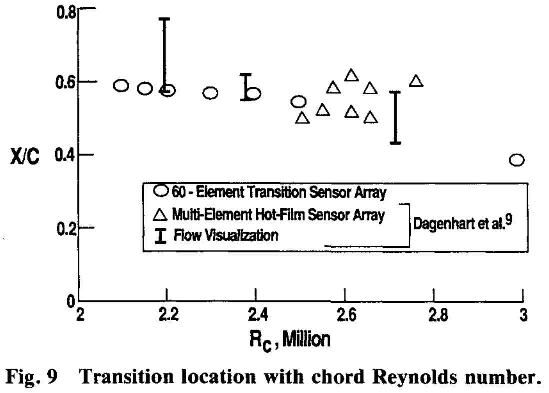

Fig. 9 Transition location with chord Reynolds number.

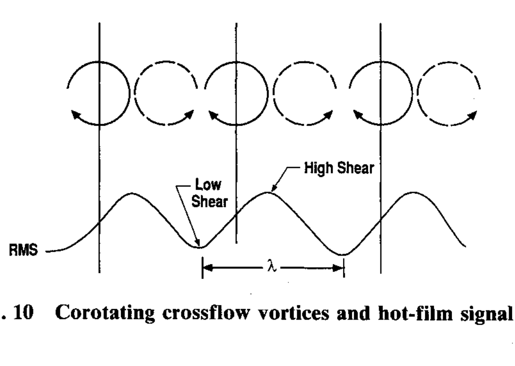

Fig. 10 Corotating crossflow vortices and hot-film signal.

Fig. 11 Simultaneously acquired signals from 33-element crossflow sensor array, $R_c = 2.80 \times 10^6$, $X/C = 0.40$.

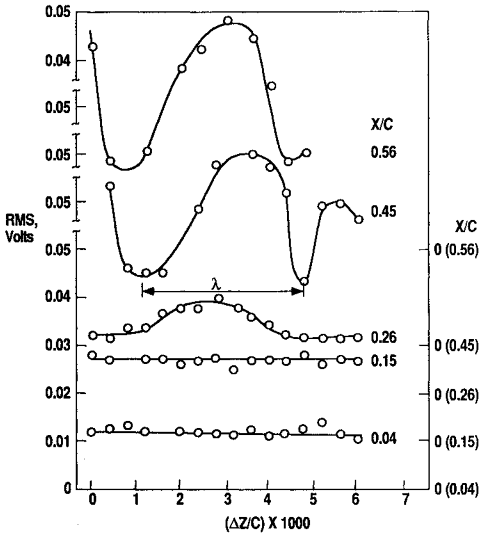

Fig. 12 Spanwise crossflow vortex development with varying chord location (rms from 64-element crossflow sensor arrays), $R_c = 2.5 \times 10^6$. Solid lines for visual aid only.

In the present experiment, crossflow wavelengths were obtained from 16 spanwise measurements. Figure 11 shows hot-film signals in the spanwise direction at $X/C = 0.4$ and $R_c = 2.8 \times 10^6$ using a 33-element crossflow gauge. Sensor signals at locations $\Delta Z/C = 0.0008$ and 0.0017 show laminar flow. Low-frequency spikes appear at $\Delta Z/C = 0.0025$. Spike frequencies increase for sensors between $\Delta Z/C = 0.0034$ and 0.0050 and then decrease for sensors at $\Delta Z/C = 0.0059$ and 0.0067. It is evident from Fig. 11 that the boundary-layer flow in the presence of crossflow vortices is highly three-dimensional. These sensors are nominally at the same chord location but have a marked difference in their turbulent burst pattern; this occurs even though the spacing between crossflow sensors is only 0.75 mm (alternate sensors are shown in Fig. 11).

Development of crossflow vortices along the chord and span is shown in Fig. 12, where the rms variation of hot-film signals (from the 64-element crossflow sensor arrays as shown in Fig. 5) in the spanwise direction is shown at $X/C = 0.04$, 0.15, 0.26, 0.45, and 0.56 at $R_c = 2.5 \times 10^6$. At $X/C = 0.04$ and 0.15, any spanwise variation in rms is obscured by the low signal. At $X/C \geq 0.26$, the crossflow vortices are well devel-

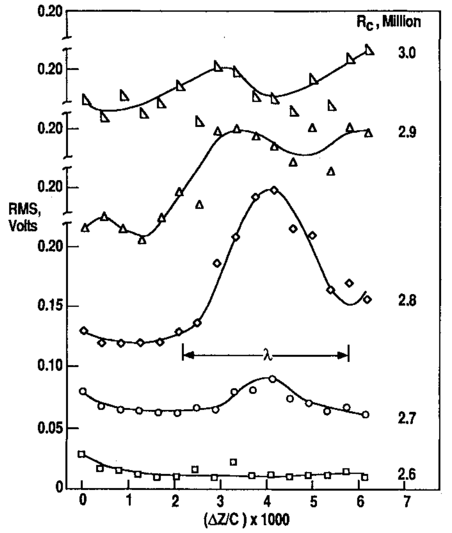

Fig. 13a Spanwise crossflow vortex development with varying Reynolds number (rms from 33-element crossflow sensor arrays), $X/C = 0.40$. Solid lines for visual aid only.

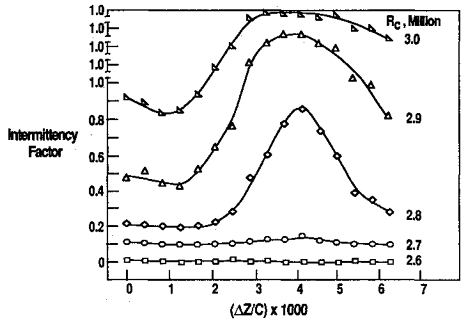

Fig. 13b Spanwise crossflow vortex development with varying Reynolds number (intermittency factor from 33-element crossflow sensor arrays), $X/C = 0.40$. Solid lines for visual aid only.

oped and the rms variation clearly shows a peak and two valleys. The difference in rms at two minima can be attributed to the different level of fluctuations at two different X/C locations. The minimum locations at different chordwise stations are not exactly aligned because only 16 of the 64 crossflow sensors were used (which were not at exactly the same spanwise position for various chord locations). The vortex wavelength λ, the distance between two minima, is nearly the same for $X/C = 0.26$, 0.45, and 0.56. The flow at $X/C = 0.56$ (for the spanwise locations shown in Fig. 12) is not turbulent, whereas Fig. 9 at a different spanwise location shows turbulent flow near $X/C = 0.56$. This is due to the sawtooth pattern of the flow transition over the wing (as shown by flow visualization studies; refer to Fig. 5). Transition measurements shown in Fig. 9 are at one spanwise location only.

Figure 13a shows the rms variation at $X/C = 0.4$ and at five different Reynolds numbers from 2.6 to 3.0×10^6. At $R_c = 2.6 \times 10^6$, signal levels are small. A vortex structure appears at $R_c = 2.7 \times 10^6$, and is well defined at $R_c = 2.8 \times 10^6$. At $R_c = 2.9$ and 3.0×10^6, the turbulent vortex is diffused. The flow intermittency factor for the Fig. 13a data is shown in Fig. 13b. Intermittency factor plots show the same trend. For the first three cases, the intermittency factor at the peak rms location is well below 1.

The crossflow vortex wavelength obtained from the data presented in Figs. 13a and 13b and other similar data is presented in Figs. 14a and 14b. Results are in good agreement with the flow-visualization results of Dagenhart et al.[9] Figure 14a also shows that the crossflow vortex wavelength decreases with increased chord Reynolds number (chord Reynolds number was varied by changing the tunnel speed). Reduced λ as R_c increases is probably due to the reduced boundary-layer thickness with increased R_c. The data of Fig. 14a replotted in Fig. 14b show that, within experimental accuracy, the crossflow vortex wavelength does not vary significantly with chord in the range $0.4 \leq X/C \leq 0.56$, as also observed by the flow visualization. Arnal[4] and Arnal and Juillen[7] have measured a growing wavelength with chord on a long swept wing in an open-jet wind tunnel: flow conditions in that experiment are different from the present experiment, which may cause a different crossflow vortex pattern. Measurements made here agree with the results of Dagenhart et al.[9] using the same facility.

Nonstationary Crossflow Disturbance

Leading-edge wing sweep at high Reynolds number causes instability in laminar boundary-layer flow. In addition to stationary disturbances, this instability also develops traveling

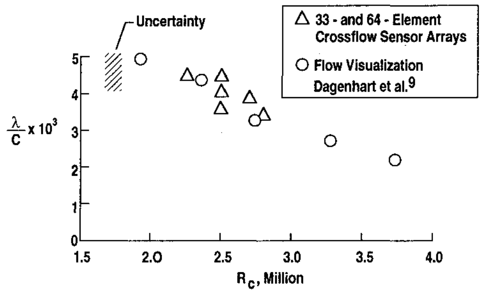

Fig. 14a Crossflow vortex wavelength variation (from 33- and 64-element crossflow sensor arrays) with chord Reynolds number.

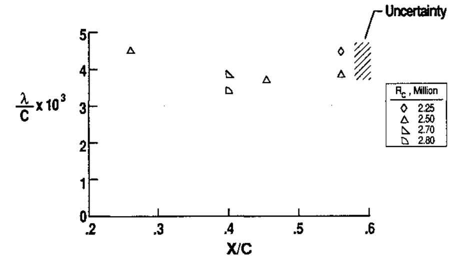

Fig. 14b Crossflow vortex wavelength variation (from 33- and 64-element crossflow sensor arrays) with chordwise distance.

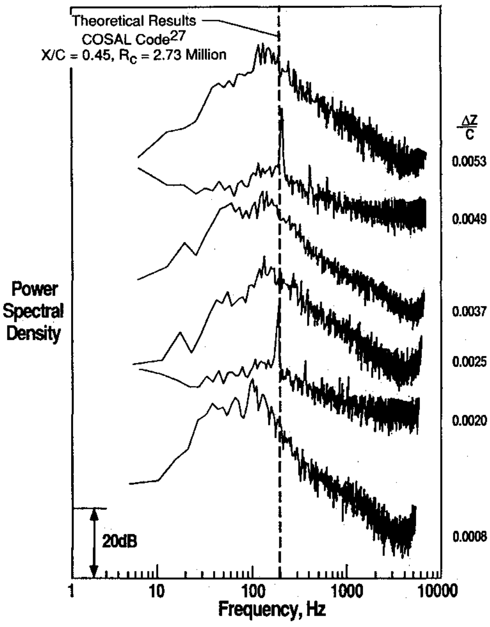

Fig. 15 Spanwise power spectral density from 64-element crossflow sensor arrays, $R_c = 2.5 \times 10^6$, $X/C = 0.45$.

harmonic waves. In the present experiment, nonstationary disturbances were observed at all of the chordwise measurement locations. The frequencies of these disturbances were obtained from the discrete peaks in the spectral density plots. Near transition, because of higher spectral densities due to the turbulent nature of the flow, it was difficult to identify the disturbances by this method. Figure 15 shows the spectral density variation in the spanwise direction at $X/C = 0.45$. At $\Delta Z/C = 0.0020$ and 0.0049, where rms levels are low (refer to Fig. 12 where the spanwise rms of this signal variation is shown), crossflow disturbance frequencies are marked by sharp spectral peaks. The most amplified crossflow disturbance frequency from linear stability theory, using the COSAL code[27] at nearly the same Reynolds number and chordwise location, is also shown in Fig. 15. The disturbance frequency as shown by spectral peaks at $\Delta Z/C = 0.0020$ and 0.0049 is in good agreement with the most amplified frequency predicted by theory.

The variation of the crossflow disturbance frequencies in the spanwise direction at $X/C = 0.04$, 0.15, 0.26, 0.45, 0.56, and 0.67 are shown in Figs. 16a–16c. It is clear from these figures that the crossflow disturbance frequencies are constant in the spanwise direction. Disturbance frequencies shown in these figures were obtained by spectral analysis of hot-film signals. The frequencies shown correspond to all of the peaks in the spectra. Although several harmonics of crossflow disturbance frequency are present in the spectrum, only one is the most amplified crossflow disturbance frequency at a given chord location. Since the hot films were not calibrated, it was not possible to identify the most amplified disturbance frequencies from the several sets of amplified disturbances present at a given chordwise location.

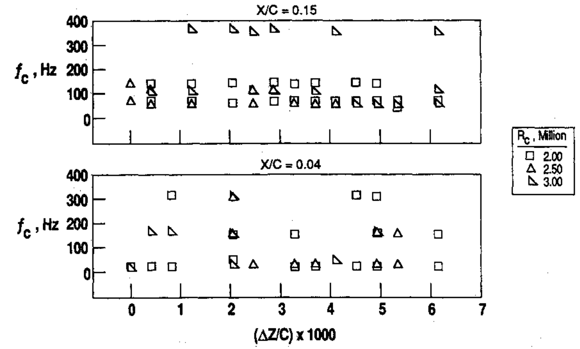

Fig. 16a Spanwise variation of crossflow disturbance frequencies from 64-element crossflow sensor arrays, $X/C = 0.04$ and 0.15.

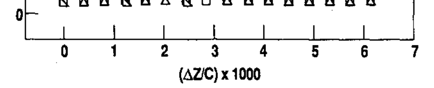

Fig. 16b Spanwise variation of crossflow disturbance frequencies from 64-element crossflow sensor arrays, $X/C = 0.26$ and 0.45.

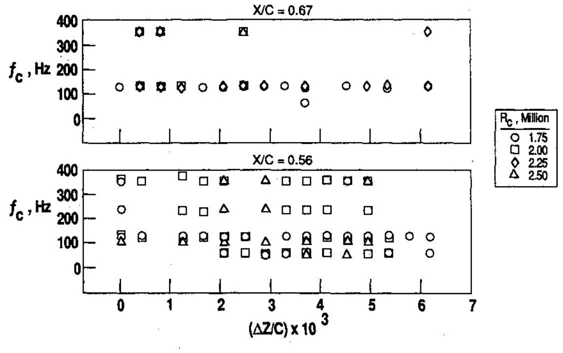

Fig. 16c Spanwise variation of crossflow disturbance frequencies from 64-element crossflow sensor arrays, $X/C = 0.56$ and 0.67.

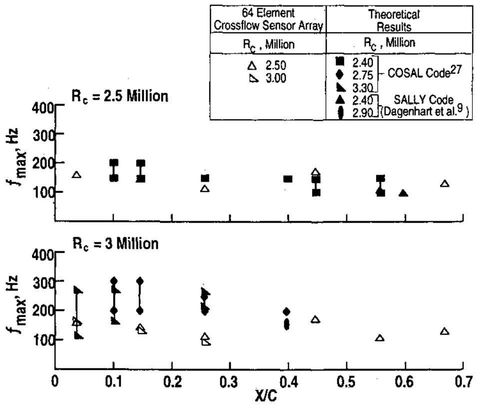

Fig. 17 Chordwise variation of crossflow disturbance frequencies (64-element sensor arrays and theoretical results).

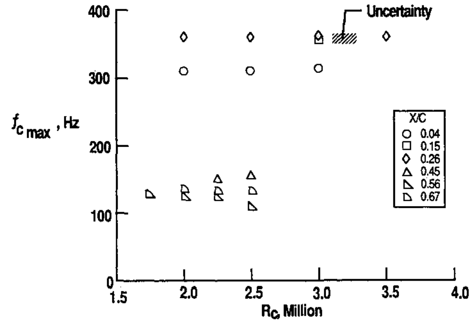

Fig. 18 Most amplified crossflow disturbance frequencies from 64-element crossflow sensor arrays with Reynolds number.

Measured amplified frequencies at various chordwise locations and two Reynolds numbers, and theoretical results from the COSAL code[27] and from Dagenhart et al.[9] using the SALLY code (at Reynolds numbers close to the experimental results), are shown in Fig. 17. All of the crossflow disturbance frequencies from the spectral analysis are shown. Most amplified crossflow disturbance frequencies can be inferred from Fig. 17, where the measurements are compared with the theoretical results. Figure 17 shows that the most amplified disturbance frequencies decrease in chord direction. Most amplified crossflow disturbance frequencies at six chord locations (from Figs. 16 and 17) are shown in Fig. 18. Within the range of chord Reynolds number, the most amplified crossflow disturbance frequencies at a given X/C do not significantly vary.

At $X/C = 0.45$ (Fig. 16b), a disturbance frequency of about 850 Hz is observed, much higher than predicted by theory at this chord location. Mangalam et al.[12] (from measurements on the same model) also observed amplified disturbances near 1 kHz at $X/C = 0.4$. The reason for the presence of this higher frequency amplified disturbance has not been established.

Conclusions

An experiment was conducted on a 45-deg swept-wing model to study crossflow vortex structure and transition. Simultaneous measurements were obtained from surface-mounted, microthin, multielement hot-film sensors. The measurements show that transition occurred ahead of the pressure minimum (which was at $X/C = 0.71$) for Reynolds number $\geq 2.15 \times 10^6$. The transition process appears to be initiated by crossflow disturbances.

Stationary crossflow vortices were seen by flow-visualization methods on the wing surface. The crossflow vortex structure and wavelength obtained from the spanwise rms variation agree with flow-visualization results.

Nonstationary crossflow disturbance frequencies were obtained from simultaneous measurements using hot-film sensors located in both chordwise and spanwise directions. The most amplified crossflow disturbance frequencies decreased with distance along the chord and showed good agreement with linear stability theory.

Acknowledgments

The authors would like to thank W. S. Saric of Arizona State University for the use of the wind tunnel and his support during the experimental program and J. Ray Dagenhart, NASA Langley Research Center, for his valuable comments on the sketch of the crossflow vortex structure. Thanks are also due to R. Putnam and R. Rowe of Lockheed Engineering & Sciences Company for their help in the data reduction and preparation of the figures.

References

[1] Pfenninger, W., "Flow Phenomenon at the Leading Edge of Swept Wings," AGARDograph 97, May 1965.

[2] Reed, H. L., and Saric, W. S., "Stability of Three-Dimensional Boundary Layers," *Annual Review of Fluid Mechanics,* Vol. 21, 1989, pp. 235–284.

[3] Saric, W. S., "Boundary-Layer Transition: T-S Waves and Crossflow Mechanisms," AGARD Rept. No. 723, 1985.

[4] Arnal, D., "Three-Dimensional Boundary Layers: Laminar-Turbulent Transition," AGARD Rept. No. 741, 1986.

[5] Saric, W. S., and Yeates, L. G., "Experiments on the Stability of Crossflow Vortices in Swept Wing Flows," AIAA Paper 85-0493, Jan. 1985.

[6] Bippes, H., and Nitschke-Kowsky, P., "Experimental Study of Instability Modes in a Three-Dimensional Boundary Layer," AIAA Paper 87-1336, June 1987.

[7] Arnal, D., and Juillen, J. C., "Three-Dimensional Transition Studies at ONERA/CERT," AIAA Paper 87-1335, June 1987.

[8] Muller, B., and Bippes, H., "Experimental Study of Instability Modes in a Three-Dimensional Boundary Layer," AGARD CP-438, Çeşme, Turkey, Oct. 1988.

[9] Dagenhart, J. R., Saric, W. S., Mousseux, M. C., and Stack, J. P. "Crossflow-Vortex Instability and Transition on a 45-Degree Swept Wing," AIAA Paper 89-1892, June 1989.

[10] Kohama, Y., "Some Expectation on the Mechanism of Crossflow Instability in a Swept Wing Flow," *Acta Mechanica,* Vol. 66, 1987, pp. 21–38.

[11] Poll, D. I. A., "Some Observations of the Transition Process on the Windward Face of a Long Yawed Cylinder," *Journal of Fluid Mechanics,* Vol. 150, 1985, pp. 329–356.

[12] Mangalam, S. M., Maddalon, D. V., Saric, W. S., and Agarwal, N. K., "Measurements of Crossflow Vortices, Attachment-Line Flow, and Transition Using Microthin Hot Films," AIAA Paper 90-1636, June 1990.

[13] Saric, W. S., Takagi, S., and Mousseux, M., "The ASU Unsteady Wind Tunnel and Fundamental Requirements for Free-Stream Turbulence Measurements," AIAA Paper 88-0053, Jan. 1988.

[14] Holmes, B. J., Croom, C. C., Gall, P. D., Manuel, G. S., and Carraway, D. L., "Advanced Transition Measurements Methods for Flight Applications," AIAA Paper 86-9786, April 1986.

[15] Holmes, B. J., Carraway, D. L., Manuel, G. S., and Croom, C. C., "Advanced Measurement Techniques," *Proceedings of Research in Natural Laminar Flow and Laminar Flow Control,* NASA CP-2487, 1987.

[16] Johnson, C. B., Carraway, D. L., Hopson, P., Jr., and Tran, S. Q., "Status of a Specialized Boundary-Layer Transition Detection System for Use in the U.S. National Transonic Facility," *Proceedings of 12th International Congress in Instrumentation in Aerospace Simulation Facilities,* Williamsburg, VA, June 1987.

[17] Johnson, C. B., and Carraway, D. L., "A Transition Detection Study at Mach 1.5, 2.0, and 2.5 using a Micro-Thin Hot-Film System," 13th International Congress in Instrumentation in Aerospace Simulation Facilities, Gottingen, Germany, Sept. 1989.

[18] Stack, J. P., Mangalam, S. M., and Berry, S. A., "A Unique Measurement Technique to Study Laminar-Separation Bubble Characteristics on an Airfoil," AIAA Paper 87-1271, June 1987.

[19] Mangalam, S. M., Stack, J. P., and Sewall, W. G., "Simultaneous Detection of Separation and Transition in Surface Shear Layers," AGARD CP-438, Çeşme, Turkey, Oct. 1988.

[20] Narasimha, R., "The Laminar-Turbulent Transition Zone in the Boundary Layer," *Progress in Aerospace Sciences,* Vol. 22, 1985, pp. 29–80.

[21] Gray, W. E., "The Effect of Wing Sweep on Laminar Flow," Royal Aircraft Establishment, Rept. No. TM Aero. 255, Farnborough, England, UK, Feb. 1952.

[22] Gray, W. E., "The Nature of Boundary Layer Flow at the Nose of a Swept Wing," Royal Aircraft Establishment, Rept. No. TM Aero. 256, Farnborough, England, UK, June 1952.

[23] Mack, L. M., "Boundary-Layer Linear Stability Theory," AGARD Rept. No. 709, 1984.

[24] Malik, M. R., and Poll, D. I. A., "Effect of Curvature on Three-Dimensional Boundary Layer Stability," AIAA Paper 84-1672, June 1984.

[25] Michel, R., Arnal, D., Coustols, E., and Juillen, J. C., "Experimental and Theoretical Studies of Boundary Layer Transition on a Swept Infinite Wing," *Proceedings of the Laminar-Turbulent Transition Symposium,* Novosibirsk, Russia, July 1984, Springer-Verlag, pp. 553–561.

[26] Reed, H. L., "Wave Interactions in Swept-Wing Flows," *Physics of Fluids,* Vol. 30, No. 11, 1988, pp. 3419–3426.

[27] Malik, M. R., "COSAL—A Black Box Compressible Stability Analysis Code for Transition Prediction in Three-Dimensional Boundary Layers," NASA-CR 165925, May 1982.